JULY, 2013

Theoretical study on the fragmentation dynamics of L-Alanine^{2+}

Estefanía Rossich Molina

Master Thesis

European Master in
Theoretical Chemistry and Computational Modelling

JULIO, 2013

Estudio teórico de la dinámica de la fragmentación de la L-Alanina^{2+}

Estefanía Rossich Molina

Tésis de Máster

Máster europeo en
Química Teórica y Modelización Computacional

D. Ángel Martín Pendás, Catedrático del Departamento de Química Física y Analítica de la Universidad de Oviedo y Coordinador del Máster Europeo en Química Teórica y Modelización Computacional,

CERTIFICA:

Que el trabajo titulado **Estudio teórico de la dinámica de la fragmentación de la L-Alanina^{2+}** ha sido realizado por Estefanía Rossich Molina, bajo la tutela del catedrático D. Yang Wang con el fin de optar al título que otorga el Máster Europeo en Química Teórica y Modelización Computacional.

Oviedo, 15 de julio de 2013

Fdo.: Ángel Martín Pendás
Coordinador del Máster Europeo en Química Teórica y Modelización Computacional

D. Ángel Martín Pendás, Catedrático de Química Física del Departamento de Química Física y Analítica de la Universidad de Oviedo,

CERTIFICA:

Que el trabajo titulado **Estudio teórico de la dinámica de la fragmentación de la L-Alanina^{2+}** , ha sido realizado bajo su dirección por Estefanía Rossich Molina, constituyendo su Tésis de Máster, cuya presentación autoriza.

Oviedo, 15 de julio de 2013

Fdo.: Ángel Martín Pendás

Agradecimientos

Antes que nada, quiero agradecer a Yang Wang y Angel Pendás, por su paciencia y tiempo dedicado a enseñarme y seguir mi trabajo día a día.

Además, gracias a Manuel Alcamí y Fernando Martín que me dieron la oportunidad de realizar este máster y siempre estuvieron dispuestos cuando necesité apoyo. Desde su experiencia supieron aconsejarme y hacerse tiempo en sus complicadas agendas para atender cualquier inquietud.

También ha sido importante para la realización de esta tesis, contar con resultados experimentales. Por eso agradezco a la gente que integra el grupo de colaboración en la Universidad de Turku, Finlandia (Dang Trinn Ha, Edwin Kukk) y al Max-Lab en Suecia donde se realizaron los experimentos.

Gracias al departamento de Química y al Centro de Computación de la Universidad Autónoma de Madrid y Xchem por darme los recursos para realizar mis cálculos.

Gracias a Wilson y Beatriz por todo su trabajo.

Pasando de lo académico a lo personal, gracias a mi familia, gracias por apoyarme siempre. Gracias a mis amigos del máster en Madrid porque estando lejos de mi país, son ellos quienes se convirtieron en mi familia en España y hacen que me sienta muy a gusto. En especial a Lara y Oriana, a la gente del “501-A”. Con ellos compartí mis días en un ambiente de trabajo inmejorable. Gracias por cada intercambio de ideas en la pizarra, por cada almuerzo compartido, por cada momento de colaboración sin importar la hora del día ni el día de la semana.

Por último, gracias a las personas del máster en otras universidades del consorcio, porque compartir con ellos ha sido para mí sin dudas una de las experiencias más enriquecedoras tanto académica como culturalmente y aunque el tren nos va llevando a cada uno por distintos caminos, estoy feliz de haberlos conocido.

Abstract

X-rays are used with both diagnostic and therapeutic (cancer treatment) objectives. The time scale of the fragmentations of biomolecules that may occur after being radiated with X-rays is around 1 to 100 fs. These values are so small that one cannot establish the mechanism of these processes by experimental studies. So, another approach is needed and molecular dynamics (MD) simulations have shown to be successful for this purpose.

Co-workers from an experimental group in Turku University have recently performed experiments with X-radiation to ionize the L-alanine. This ionization step leads to fragments which time of flights (ToFs) are recorded in a PEPIPICO (photo-electron photo-ion photo-ion coincidence map).

In the present work, we tackle the study of fragmentation of L-alanine^{2+} in gas phase. We begin with the theoretical study on the energy barriers for different fragmentation channels. Then, using Car-Parrinello MD (CP MD) we study the thermal dissociation. In this method we assume that the Born-Oppenheimer approximation is valid. It means that we work under adiabatic conditions.

Finally, for processes in excited states we resort to the use of time dependent density functional theory molecular dynamics (TD-DFT MD). Here we prepare an initial doubly charged state by removing two electrons from a particular inner Kohn-Sham orbital of the neutral molecule. The system evolves according to the Ehrenfest MD approximation. The mean-field potential energy surface (PES) which drives nuclear dynamics is computed at the TD-DFT level, propagating time-dependent Kohn-Sham orbitals. Nuclear forces are computed using the Hellmann-Feynman theorem.

DFT calculations at the BLYP/6-311++G(d,p) level of theory show that the fragmentations of doubly charged L-Alanine on C-C bonds have energy barriers and the dissociation leads to two singly charged fragments.

From our CP MD simulations, we found that the critical temperature for the thermal fragmentation of L-alanine is 1900 K. Two fragmentation channels are distinguished depending on the temperature used for the simulations: below 11254 K the fragmentation leads to two singly charged fragments: COOH and $CH_3CH(NH_2)$ with masses 45/44 respectively. Above 11254 K, two singly charged fragments are produced: COOH, H_2CCH_2 which masses are 45/28 and a neutral fragment, NH_2 (mass 16). Both fragmentation channels are supported by experimental PEPIPICO results.

TD-DFT MD simulations give other interesting results that are not found using the CP MD in ground state. H_3C— $CH(NH_2)COOH$ bond breaks leading to a CH_3 fragment observed in PEPIPICO map. Continuing this simulation we expect further dissociation as supported by this mentioned PEPIPICO path.

Contents

Chapter 1. INTRODUCTION

Since light, or electromagnetic radiation, covers a huge range of energies corresponding to wavelengths from 10^{12} nm to 10^{-3} nm, it should not be surprising that different phenomena can take place when it interacts with matter. Although scientists have been investigating on this area for centuries, there is still too much to know about the light-matter interaction.

Among all these phenomena, in the present thesis we deal with the photo absorption of X-ray. The absorption of light can change bond lengths, lead to isomerization processes and molecular fragmentation. The latter one is the process that we study here.

Throughout the last fifty years the growth has been remarkable in the development of technology of synchrotron radiation and this boosted the study on the phenomena of absorption of light ranging from vacuum ultraviolet (VUV) to X-ray. Furthermore, X-rays are used to treat different kind of cancer and also as a diagnostic technique. These medical applications have been probed to have undesired side effects, (e.g., *in utero* exposure to this radiation in diagnostic doses was probed to increase subsequent mortality from neoplastic disease during childhood, (***1***) and for patients for tuberculosis, who have been practiced frequent chest X-Ray fluoroscopy, showed a higher breast cancer incidence) (***2***), that make the understanding of the interaction between X-ray and biological molecules an important research area. It is not yet known exactly how a certain amount of energy supplied to a molecular system cause it to be fragmented in a certain way or another, One of the reasons is that the more degrees of freedom a molecular system has, the larger variety of possible dissociation channels it may possess, so it is difficult to understand and describe the whole process in detail. Even more, the less likely patterns when studied in experiments often give poor signals that are not easy to be distinguished from background noise. This means that the measurements in general show only a distribution of the most probable channels.

In this study, we have chosen an amino acid (AA) molecule: L-alanine ($C_3H_7NO_2$) as a biomolecule model. It is a non-essential AA synthesized in human body and it has several biologic functions, e.g. Cahill cycle (***18***). As we see in Fig. (1.1), L-alanine is a small molecule with no aromatic rings so it is supposed to be easy to dissociate.

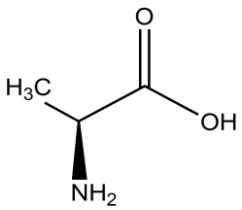

Fig. 1.1: L-alanine structure.

The apparatus used in experiments is described thoroughly in references: (***3-5***). We show it in the Fig. (1.2).

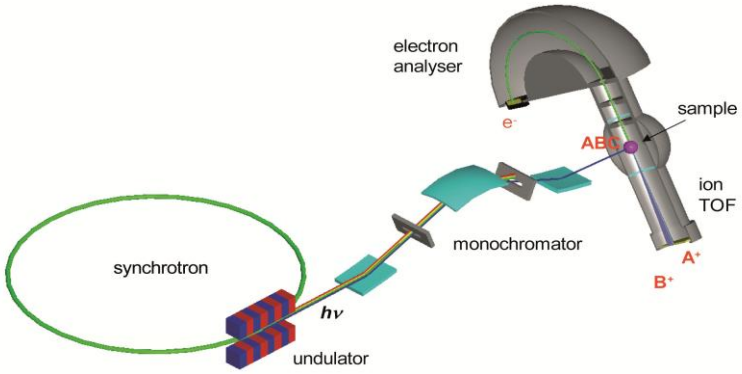

Fig. 1.2: Apparatus used for experiments.

Briefly, this experimental approach consists on incising the molecule with X-rays, then the charged fragments produced in the collision are mass-to-charge (M/Z) analyzed by means of a time-of-flight (TOF) mass spectrometer. The TOF of all fragments created by one pulse is measured by a multistep time device and stored in an event-by-event mode. This scheme allows to obtain PEPIPICO maps (photoelectron-photo-ion photo-ion coincidence maps(***6-9***)), where each signal corresponds to the TOFs of fragments produced in one particular fragmentation event. In Fig. (1.3) we see the PEPIPICO map for L-alanine.

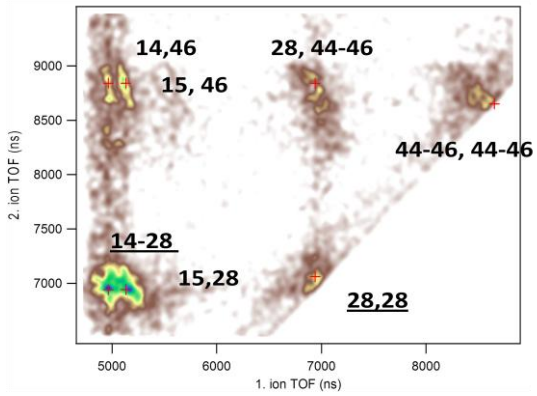

Fig. 1.3: PEPIPICO map for L-alanine.

In this context, the theoretical calculations are a fundamental tool that allows to predict and to interpret the results of this new generation of experiments. The main goal of this thesis is to go inside the interpretation, at a molecular level, of the different physical and physic-chemical phenomena occurring in the system –biological molecule- during the first ~100 fs after the ionization process with synchrotron radiation (we do not intend to describe the collisional process or the dynamics involved in the Auger

decay).

We have employed two kinds of molecular dynamics methods, time-dependent density functional theory molecular dynamics (TD-DFT MD) and Car Parrinello molecular dynamics (CP MD). In TD-DFT MD simulations effective molecular orbitals are propagated in time ***(10-11)*** to account for non-adiabatic effects in the fragmentation arising from inner-shell vacancies. The CP MD is used to study fragmentation associated with HOMO vacancies from the very first instant after ionization and thermal equilibration. The main idea of the method is that the Kohn-Sham orbitals (***12***) that describe the electronic state of a system within the density-functional theory (DFT) are evolved simultaneously with the ions as classical degrees of freedom (***13***). These approaches were used in previous works shown to be successful in a large amount of systems ***(14-17)*** .

The chapters in this thesis are organized such that the second one, after the present introduction section, describes foundations of the methodology. It begins with the description of density functional theory (DFT) and then we introduce molecular dynamics, explaining also how to get macroscopical information from the theoretical simulations. We give a setup to both CP MD and TD-DFT MD simulations. Then we explain the computational details and hypothesis assumed in our simulations.

In Chapter 3, we present the results: first we summarize results from non-dynamical studies, then the results from CP MD simulations compared with experimental results, and finally the results from TD-DFT MD simulations. In Chapter 4 we have drawn the most important conclusions. And the last Chapter corresponds to the future work.

Chapter 2. METHODOLOGY

2.1 Density Functional Theory

There are different ways of solving Schrödinger equation. One of them is Hartree-Fock (HF) method, based on variational theorem, widely used and starting point for other techniques that include electron correlation. Another one is density functional theory (DFT) which is a conceptually different methodology based on the energy and electron density of a chemical system.

In DFT approach, the main concept is that the energy *E* of many electrons system can be expressed as a functional of the one-electron density $n(\boldsymbol{r})$. The functional $E[n]$ gives the electronic energy of the ground state.

In an *N* electron system described by the wave function $\Psi(x_1, \ldots, x_N)$, the probability of finding an electron 1 in the interval [x_1,x_1+dx] and an electron 2 in the interval [x_2,x_2+dx] et cetera, is given by the product:

$$\Psi(x_1, \ldots, x_N)\Psi^*(x_1, \ldots, x_N)dx_1 \ \ldots, dx_N \tag{2.1}$$

On the other hand, the probability of finding an electron 1 in the interval [x_1,x_1+dx] independently of the localization of the other electrons is expressed by:

$$dx_1 \int \Psi\ (x_1, \ldots, x_N)\Psi^*(x_1, \ldots, x_N)dx_1 \ \ldots, dx_N \tag{2.2}$$

As the electrons are indistinguishable,

$$n(x_1)dx_1 = Ndx_1 \int \Psi\ (x_1, \ldots, x_N)\Psi^*(x_1, \ldots, x_N)dx_1 \ \ldots, dx_N \tag{2.3}$$

Integrating respect the spin coordinates we arrive to the expression of the electronic density, noted $n(\boldsymbol{r})$. The electronic density gives the number of electrons per unit of volume. So, considering the electron charge, and making the product by the number of electrons we can obtain the electron density.

$$n(r_1) = \int n(x_1)ds_1 \tag{2.4}$$

$$n(r_1) = N \int \Psi\ (x_1, \ldots, x_N)\Psi^*(x_1, \ldots, x_N)ds_1 \ \ldots, ds_N \tag{2.5}$$

Finally, considering that Ψ is normalized:

$$\int n(\mathbf{r})d\mathbf{r} = N \tag{2.6}$$

We cannot measure the wavefunction, but is possible to measure the electronic density. Independent of the size of the molecule, the electron density is always a function of three variables while the wavefunction becomes more and more complex.
The average electronic energy can be expressed as a functional of the ground state electron density:

$$E[n] = T[n] + V_{Ne}[n] + V_{ee}[n] \tag{2.7}$$

The first contribution to the average electronic energy is the average kinetic electron energy, the second is the average nuclear-electron attraction energy and the last, average electron-electron repulsion energy.

If the system is a closed-shell one:

$$\hat{V}_{Ne} = -\sum_{\alpha=1}^{N}\sum_{i=1}^{n}\frac{Z_\alpha}{r_{\alpha i}} = \sum_{i=1}^{n} v(r_i) \tag{2.8}$$

$v(r_i)$ is the external potential created by all the nuclei on the i^{th}-electron.
Taking into account the nuclear-electron potential:

$$V_{Ne}[n] = \int n(\boldsymbol{r})\, v(\boldsymbol{r})\, d\boldsymbol{r} \tag{2.9}$$

and the definition of Hohenberg-Kohn functional:

$$F_{HK}[n] = T[n] + V_{ee}[n] \tag{2.10}$$

And replacing equations (2.9) and (2.10) the equation (2.7):

$$E[n] = \int n(\boldsymbol{r})\, v(\boldsymbol{r})\, d\boldsymbol{r} + F_{HK}[n] \tag{2.11}$$

Hohenberg-Kohn theorems

The two Hohenberg-Kohn theorems are the base for DFT.

The first theorem states a relation one-to-one between an external potential $v(\boldsymbol{r})$ and a non- degenerated wavefunction $|\Psi_0(\boldsymbol{r})\rangle$ and between the latter one and a unique $n_0(\mathbf{r})$. Esquematically:

$$v(\boldsymbol{r}) \rightleftarrows |\Psi_0(\boldsymbol{r})\rangle \rightleftarrows n_0(\mathbf{r}) \tag{2.12}$$

In this way, all the properties of the ground state of a system are determined by the ground-state density function $n_0(\mathbf{r})$.

The second theorem, establishes that the energy of any trial electron density

function $E[n_{prob}]$ and the ground state energy $E_0[n_0]$ will satisfy the following relation:

$$E[n_{prob}] \geq E_0[n_0] \tag{2.13}$$

The second theorem shows that if we choose different densities, that one which provides lower energies, will be closer to the correct one.

Kohn-Sham equations

According to the second HK theorem, minimizing the equation (2.11) we can find the ground state, but is not easy because we do not know the relationship between the density and the HK functional. The aim of Kohn-Sham method is to consider an auxiliary system of N non-interacting electrons and in this way estimate a kinetic energy of the real system, which electrons have interactions.

For n non-interacting electrons moving under an external potential, we have the Hamiltonian:

$$\widehat{H}_s = \sum_{i=1}^{n} \hbar_s(\mathbf{i}) = -\frac{1}{2}\sum_{i=1}^{n} \nabla^2(\mathbf{i}) + \sum_{i=1}^{n} \upsilon_s(\mathbf{i}) \tag{2.14}$$

Where the wavefunction of the system will be the Slater determinant constructed from the KS orbitals occupied:

$$|\Psi_s(\boldsymbol{r})\rangle = (n!)^{1/2} \,|\, \psi_1(\boldsymbol{r})\, \bar{\psi}_1\,(\boldsymbol{r}) \ldots \psi_N(\boldsymbol{r})\bar{\psi}_N\,(\boldsymbol{r})\rangle \tag{2.15}$$

Here, each KS orbital is noted as $|\psi_i(\boldsymbol{r})\rangle$ and supposing a closed shell system, we have that the density is:

$$n_s(\boldsymbol{r}) = \sum_{i=1}^{n/2} |\psi_i(\boldsymbol{r})|^2 \tag{2.16}$$

with *i* values corresponding to occupied orbitals.
The kinetic energy functional will be:

$$T_s[n_s] = -\sum_{i=1}^{n/2} \left\langle \psi_i(\boldsymbol{r}) \middle| \frac{1}{2}\nabla^2 \middle| \psi_i(\boldsymbol{r}) \right\rangle \tag{2.17}$$

Imposing the condition that the KS orbitals are chosen in such a way that is verified: $n_s(\boldsymbol{r}) = n_0(\boldsymbol{r})$, so the average electron energy now can be written as:

$$E[n] = T_s[n] + V_{Ne}[n] + V_{ee}[n] + \Delta T[n] + \Delta V_{ee}[n] \tag{2.18}$$

We have already said that $T_s[n]$ is the kinetic energy for a non-interacting system

and $V_{Ne}[n]$, the nuclear-electron interaction. $V_{ee}[n]$ is the classical electrostatic repulsion energy. These three terms can be calculated if we know the set of KS spin-orbitals $\{|\psi_i\rangle\}$.
The exchange-correlation functional,

$$E_{XC}[n] = \Delta T[n] + \Delta V_{ee}[n] \tag{2.19}$$

includes the other two terms involving quantities that are not known: $\Delta T[n]$ includes deviations of the real kinetic functional from the reference system, and $\Delta V_{ee}[n]$, the corrections to electron classical self-interaction.

Finally we arrive to a equation that, if we know the $E_{XC}[n]$, is exact. Is called Kohn Sham energy equation:

$$E[n] = T_s[n] + \int n(\boldsymbol{r})v(\boldsymbol{r}) + \frac{1}{2}\int\int \frac{n(\boldsymbol{r}_1)n(\boldsymbol{r}_2)}{r_{12}}\, d\boldsymbol{r}_1 d\boldsymbol{r}_2 + E_{XC}[n] \tag{2.20}$$

but we have mentioned before that this is the problem with DFT, we do not know the exchange correlation energy functional. Its dependence with on the electron density is expressed as an interaction between the energy density functional $\epsilon_{XC}[n]$ and the electron density n(**r**):

$$E_{XC}[n] = \int n(\boldsymbol{r})\epsilon_{XC}[n]d\boldsymbol{r} \tag{2.21}$$

Here we face with a weak point of the theory: we do not know which is the exact relation between the electronic density and the functional, so we have to find a suitable approximation for the functional in order to be applied to any one-electron density. This means, there is no way to systematically improve the functional and the choice of the functional determines whether a calculation will success or not.

The Born-Oppenheimer approximation

The Born-Oppenheimer (BO) approximation emerges from the fact that the mass of the nuclei are over 1000 times the mass of the electrons.

The time independent Kohn-Sham equation:

$$\left[\hat{T}_N(\boldsymbol{R}) + \hat{H}_e(\boldsymbol{r},\boldsymbol{R})\right]|\psi(\boldsymbol{r}|\boldsymbol{R})\rangle = E\,|\psi(\boldsymbol{r}|\boldsymbol{R})\rangle \tag{2.22}$$

where $\hat{T}_N(\boldsymbol{R})$ represents the kinetic nuclear operator and E is a real number (since $\hat{H}$ is an hermitian operator). The solutions to this equation cannot be expressed as a simple separation of electronic and nuclear variables because the molecular Hamiltonian operator depends on the two set of coordinates, it has a crossed term, $\hat{V}_{eN}(\boldsymbol{r},\boldsymbol{R})$. But considering the mass difference between electrons and nuclei, we can see the problem

as the nuclei fixed to respect to the electron movement. Therefore, if nuclei are considered fixed, nuclear coordinates act as parameters. Under this approximation the total spatial function might be expressed as a product of a electronic wavefunction and a nuclear wavefunction:

$$|\psi(\boldsymbol{r}|\boldsymbol{R})\rangle = E\ |\Psi_k(\boldsymbol{r}|\boldsymbol{R})\rangle|\chi_N(\boldsymbol{R})\rangle \tag{2.23}$$

Where the electronic wavefunction has a parametric dependency on nuclear positions. Wavefunctions like (2.23) are solutions of (2.22), i.e.:

$$\hat{H}|\Psi_k(\boldsymbol{r}|\boldsymbol{R})\rangle|\chi_N(\boldsymbol{R})\rangle = E_K|\Psi_k(\boldsymbol{r}|\boldsymbol{R})\rangle\ |\chi_N(\boldsymbol{R})\rangle \tag{2.24}$$

Or, what is the same:

$$\begin{gathered}\left\{\hat{T}_N(\boldsymbol{R}) + \hat{T}_e(\boldsymbol{r}) + \hat{V}_{eN}(\boldsymbol{r};\boldsymbol{R}) + \hat{V}_{NN}(\boldsymbol{R}) + \hat{V}_{ee}(\boldsymbol{r})\right\}|\Psi_k(\boldsymbol{r}|\boldsymbol{R})\rangle|\chi_N(\boldsymbol{R})\rangle \\ = E_K|\Psi_k(\boldsymbol{r}|\boldsymbol{R})\rangle\ |\chi_N(\boldsymbol{R})\rangle\end{gathered} \tag{2.25}$$

If the kinetic energy of the nuclei is neglected we arrive to the electronic equation:

$$\hat{H}_e(\boldsymbol{r},\boldsymbol{R})|\Psi_k(\boldsymbol{r}|\boldsymbol{R})\rangle = E_k(\boldsymbol{R})\ |\Psi_k(\boldsymbol{r}|\boldsymbol{R})\rangle \tag{2.26}$$

If we consider the nuclear motion, going back to eq. (2.25) he nuclear kinetic term is given by:

$$\begin{gathered}\hat{T}_N(\boldsymbol{R})|\Psi_k(\boldsymbol{r}|\boldsymbol{R})\rangle|\chi_N(\boldsymbol{R})\rangle = -\sum_{\alpha=1}^{N}\frac{\hbar^2}{2M_\alpha}\ |\Psi_k(\boldsymbol{r}|\boldsymbol{R})\rangle\ \nabla_\alpha^2|\chi_{\mathrm{N}}(\mathbf{R})\rangle - \\ \sum_{\alpha=1}^{N}\frac{\hbar^2}{M_\alpha}\ |\Psi_k(\boldsymbol{r}|\boldsymbol{R})\rangle\ \nabla_\alpha|\Psi_k(\mathbf{r},\mathbf{R})\rangle\nabla_\alpha|\chi_N(\mathbf{R})\rangle - \\ \sum_{\alpha=1}^{\mathrm{N}}\frac{\hbar^2}{2M_\alpha}|\chi_N(\mathbf{R})\rangle\nabla_\alpha^2|\chi_{\mathrm{N}}(\mathbf{r},\mathbf{R})\rangle\end{gathered} \tag{2.27}$$

Since $\hat{T}_e(\boldsymbol{r})$ contains no **R** dependence:

$$\hat{T}_e(\boldsymbol{r})|\chi_k(\boldsymbol{r}|\boldsymbol{R})\rangle|\Psi_N(\mathbf{R})\rangle = |\chi_N(\mathbf{R})\rangle\ \hat{T}_e\ |\Psi_k(\boldsymbol{r}|\boldsymbol{R})\rangle \tag{2.28}$$

And considering the parametric dependence:

$$\hat{V}_{eN}|\Psi_k(\boldsymbol{r}|\boldsymbol{R})\rangle|\chi_N(\mathbf{R})\rangle = |\chi_N(\mathbf{R})\rangle\ \hat{V}_{eN}\ |\Psi_k(\boldsymbol{r}|\boldsymbol{R})\rangle \tag{2.29}$$

Rearranging terms:

$$-\sum_{\alpha=1}^{N}\frac{\hbar^2}{2M_\alpha}\,|\Psi_k(\boldsymbol{r}|\boldsymbol{R})\rangle\,\nabla_\alpha^2|\chi_{\mathrm{N}}(\mathbf{R})\rangle-\sum_{\alpha=1}^{N}\frac{\hbar^2}{M_\alpha}\,\nabla_\alpha|\Psi_k(\mathbf{r},\mathbf{R})\rangle\nabla_\alpha|\chi_N(\mathbf{R})\rangle-$$
$$\sum_{\alpha=1}^{\mathrm{N}}\frac{\hbar^2}{2M_\alpha}|\chi_N(\mathbf{R})\rangle\nabla_\alpha^2|\chi_{\mathrm{N}}(\mathbf{r},\mathbf{R})\rangle+|\chi_N(\mathbf{R})\rangle\,\hat{T}_e\,|\Psi_k(\boldsymbol{r}|\boldsymbol{R})\rangle+ \quad (2.30)$$
$$\big|\chi_N(\mathbf{R})\rangle\widehat{\mathrm{V}}_{\mathrm{eN}}(\mathbf{R})|\Psi_k(\boldsymbol{r};\boldsymbol{R})\rangle+|\Psi_k(\boldsymbol{r}|\boldsymbol{R})\rangle\;\hat{V}_{NN}(\boldsymbol{R})\big|\chi_{\mathrm{N}}(\mathbf{r},\mathbf{R})\rangle+$$
$$|\chi_N(\mathbf{R})\rangle\widehat{\mathrm{V}}_{\mathrm{ee}}(\mathbf{R})|\Psi_k(\boldsymbol{r};\boldsymbol{R})\rangle=E_K|\Psi_k(\boldsymbol{r}|\boldsymbol{R})\rangle\,|\chi_N(\boldsymbol{R})\rangle$$

Second and third term can be dropped considering the mass of the nuclei much bigger than the mass of the electrons and reordering, we arrive to:

$$\left(\hat{T}_N+\left\langle\Psi_k(\boldsymbol{r};\boldsymbol{R})\middle|\hat{H}_e(\boldsymbol{r},\boldsymbol{R})\middle|\Psi_k(\boldsymbol{r};\boldsymbol{R})\right\rangle\right)|\chi_N(\boldsymbol{R})\rangle\approx E_k|\chi_N(\boldsymbol{R})\rangle \quad (2.31)$$

Due to the mass difference the molecular problem is translated to a new situation where the nuclei are moving on a PES generated by the electrons. These electrons instantaneously adjust their wavefunction according to the nuclear one. The electronic level to which corresponds the electronic wavefunction is expressed by the subindex "k". The number of electronic states is not unique for every molecule, in fact k can run from a discrete number to infinite. Linear combinations of these states can be also proposed as a solution of the TISE leading to coupling between states.

2.2 Molecular Dynamics

Molecular dynamics (MD) simulations are an important tool used since circa the end of the 50s (***19-21***) to model different types of systems: gases, liquids, solids, surfaces, clusters and biomolecules, (***22-23***) simulating at the same time both nuclei and electrons.

In the literal sense, MD is the simultaneous motion of a number of atomic nuclei and electrons forming a molecular entity. Strictly speaking, a complete description of such a system requires solving the full time-dependent Schrödinger equation including both electronic and nuclear degrees of freedom. There are several MD method and they can be classified depending on the way they use to describe the complex interactions between nuclei and electrons: classical MD simulations are based on Newton equations of motion and model potentials and the most used method inside this category is the designed as close as possible to the real system. Another category is the *ab-initio* MD, (***25***) where the nuclei are treated classically while there is used a quantum description for the electrons. Finally, the quantum MD simulations use a quantum treatment for nuclei and electrons (***26-27***). The bigger accuracy we want, the more computational resource is necessary, so to select a MD method, we need to know which information we want to obtain from the simulation.

The methods used in this thesis make a classical treatment of the nuclei and a quantum description of the electrons. They are *on-the-fly* methods: instead of calculating the whole potential energy, the potential energy is calculated at each time step based on the nuclear positions following the classical trajectory.

It is important to note that, although computer simulations are useful to study

properties of many-particle systems, not all properties can be directly measured. To calculate macroscopic properties of a real system it is convenient to define an ensemble. The general definition for an ensemble is a collection of all possible systems which has different microscopic states but have an identical macroscopic or thermodynamic attributes.

In MD simulations, we generate a sequence of points in the phase space as a function of time. These points represent microscopic states of the system and are imposed to belong to the same ensemble, in other words, they must satisfy the conditions of a particular thermodynamic state.

There are three different kinds of ensembles:

– The *canonical* ensemble (NVT): The thermodynamic state for this ensemble is characterized by a fixed number of atoms, N, a fixed volume, V, and a fixed temperature, T.

– The *grand canonical* ensemble (μVT): in this ensemble, volume, V, temperature, T and chemical potential, μ, are fixed.

– The *microcanonical* ensemble (NVE): number of atoms, N, volume, V, and energy, E are fixed.

2.3 Car-Parrinello Molecular Dynamics

In this approach, the equations of motion are integrated in the long time scale set by the nuclear motion, and takes advantage of the smooth time evolution of the dynamically evolving electronic subsystem so it does not minimize at each time-step of dynamic.

We define a Lagrangian for the electronic system as:

$$\mathcal{L} = \sum_i \mu \, \langle \dot{\psi}_i | \dot{\psi}_i \rangle - E[\{\psi_i\}, \{\boldsymbol{R}_I\}, \{\alpha_N\}] \tag{2.22}$$

In this equation μ is the fictitious mass associated to the electronic wavefunctions, E is the Kohn-Sham energy functional, $\boldsymbol{R}_I$ is the position of the ion I and α_N represents the characteristics of the unit cell: size and shape. The fictitious dynamics or the electronic degrees of freedom are responsible of the kinetic-energy term. The KS energy functional replaces the potential energy in the conventional way of formulating the Lagrangian.

Orthonormality condition must be satisfied:

$$\langle \psi_i(\boldsymbol{r}) | \psi_i(\boldsymbol{r}) \rangle = \delta_{ij} \tag{2.32}$$

And the corresponding Newton equations of motion are obtained from the associated Euler-Lagrange equations (***28***) in terms of orbitals and nuclear positions:

$$\frac{d}{dt} \frac{\partial \mathcal{L}}{\partial \dot{\boldsymbol{R}}} = \frac{\partial \mathcal{L}}{\partial \boldsymbol{R}_I} \tag{2.33}$$

$$\frac{d}{dt}\frac{\delta \mathcal{L}}{\delta \dot{\psi}_i^*} = \frac{\delta \mathcal{L}}{\delta \dot{\psi}_i^*} \tag{2.34}$$

In practice, the functional derivates in the last equation (which represent the fact that orbitals are continuous scalar fields), are represented in a basis and the concept of functional derivation reduces to the partial derivation with respect to the components of the field in the basis. Finally, we arrive at the Car-Parrinello equations of motion:

$$M_I \ddot{\boldsymbol{R}}_I(t) = \frac{\partial}{\partial \mathbf{R}_I}\left\langle \Psi_0(\boldsymbol{r}) \middle| \hat{H}_e(\boldsymbol{r}, \boldsymbol{R}) \middle| \Psi_0(\boldsymbol{r}) \right\rangle + \frac{\partial}{\partial \mathbf{R}_I} \tag{2.35}$$

$$\mu \ddot{\psi}_i(t) = \frac{\delta}{\delta \dot{\psi}_i^*}\left\langle \Psi_0(\boldsymbol{r}) \middle| \hat{H}_e(\boldsymbol{r}, \boldsymbol{R}) \middle| \Psi_0(\boldsymbol{r}) \right\rangle + \frac{\delta}{\delta \dot{\psi}_i^*} \tag{2.36}$$

2.4 Time-Dependent DFT Molecular Dynamics

We already described Car-Parrinello molecular dynamics, which is suitable for the study of the ground state. But to study excited-states we use TD-DFT molecular dynamics .TD-DFT is based on the Runge-Gross theorem that represents an extension of Hohenberg-Kohn theorem for interacting electrons under time dependent external potentials. We introduce here the basic concepts on TD-DFT: we concentrate on the time propagation of time dependent KS equations in the Ehrenfest MD.

Runge-Gross theorem

This theorem (***29***) states that for N non-relativistic electrons under a time-dependent external potential, interacting via Coulomb repulsion, the densities n(**r**,t) and n'(**r**,t) evolving from a common initial state $|\Psi_0\rangle = |\Psi_0(t=0)\rangle$ under the influence of two external potentials υ(**r**,t) y υ'(**r**,t) are always different since the potentials differ by more than a purely time-dependent (r-independent) function:

$$\upsilon(\mathbf{r}, \mathrm{t}) - \upsilon'(\mathbf{r}, \mathrm{t}) \neq c\,(t) \tag{2.37}$$

In this way it is established the bidirectional relation between densities and potentials. It means that if we only know the density of the system, is enough to know which is the external potential that produced this density, then, having the external potential we are able to solve the TDSE and obtain all the properties of the system. So, for a fixed initial state with known density, all the other properties of the quantum system are determined.

Time-Dependent Kohn-Sham equations

Kohn-Sham equations can be derived from the expression for the action potential $A[\Psi]$,

$$A[\Psi] = \int_{to}^{t} \left\langle \Psi(t) \middle| i\frac{\partial}{\partial t} - \hat{H}(\mathrm{t}) \middle| \Psi(t) \right\rangle \tag{2.38}$$

and considering an auxiliary noninteracting electrons system, under an external local potential v_{KS}.According the Runge-Gross theorem, this potential is unique and is chosen in such way that the density of the KS electrons is the same as the density of the original interacting system. So the electronic density is expressed like:

$$n(\boldsymbol{r}, t) = \sum_{n=1}^{N} |\Psi_i(\boldsymbol{r}, t)|^2 \tag{2.39}$$

Each of the non-interacting Kohn-Sham particles verifies the TDSE, this is:

$$i\frac{\partial}{\partial t}|\psi_i(\boldsymbol{r}, t)\rangle = \hat{H}_{HK}(\boldsymbol{r}, t)|\psi_i(\boldsymbol{r}, t)\rangle \tag{2.40}$$

Where $\hat{H}_{HK}(\boldsymbol{r}, t)$ is the KS Hamiltonian and $v_{KS}(\boldsymbol{r}, t)$ is the KS potential:

$$\hat{H}_{HK}(\boldsymbol{r}, t) = -\frac{1}{2}\nabla_i^2 + v_{KS}(\boldsymbol{r}, t) \tag{2.41}$$

$$v_{KS}(\boldsymbol{r}, t) = v(\boldsymbol{r}, t) + v_J(\boldsymbol{r}, t) + v_{XC}(\boldsymbol{r}, t) \tag{2.42}$$

The external potential, $v(\boldsymbol{r}, t)$, takes into account the potential created when the electron interacts with the nuclei and an applied time-dependent potential. $v_J(\boldsymbol{r}, t)$ is the time-dependent Hartree potential and the third, $v_{XC}(\boldsymbol{r}, t)$ is the exchange-correlation term representing all nontrivial many body effects. The last term is strongly dependent on the density and this relation is really complex.

The adiabatic approximation

In this approximation it is ignored the $v_{XC}(\boldsymbol{r}, t)$ dependence on density's past and instead is reduced to the instantaneous value of the density, valid if the changes in time-dependent potential are slow, or what is equivalent, if the time-dependent potential has adiabatic changes.

$$v_{XC}\,[n](\boldsymbol{r}, t) \approx v_{XC}[n(t)]\,(\boldsymbol{r}) \tag{2.43}$$

The electrons will always remain in their instantaneous ground state (GS) and spatial non-locality of the functional is given by:

$$v_{XC}\,[n](\boldsymbol{r},t) \approx v_{XC}^{GS}[n_{GS}\,(\boldsymbol{r})]_{n_{GS}(\boldsymbol{r}')=n(\boldsymbol{r}',t)} \tag{2.44}$$

Time-dependent Kohn-Sham wavefunctions: time propagation scheme

Instead of solving time-dependent KS equations to know the time-dependent KS wavefunctions, we can propagate the electronic orbitals with the linear propagator $\hat{U}(t,t_0)$ in the *time propagation scheme*:

$$|\psi_i(t)\rangle = \hat{U}(t,t_0)|\psi_i(t_0)\rangle \quad i=1,\ldots,N_e \tag{2.45}$$

where the linear propagator is:

$$\hat{U}(t,t_0) = \hat{T}_{exp}\left(-\int_{t_0}^{t}\hat{H}_{KS}(\tau)d\tau\right) \tag{2.46}$$

In this definition, τ is the Keldysh pseudotime, a way of parametrizing the time t (if the time goes from t_0 to t_1 and back to t_0, τ runs from a certain initial time, τ_i to a final time, τ_f), and $\hat{T}$ us the time ordering operator. (***30***)

The total evolution operator is divided into short segments where the Hamiltonian has a little change:

$$\hat{U}(t,t_0) = \prod_{i=0}^{N-1}\hat{U}\,\left(t_i+\Delta t_i\,,t_i\right) \tag{2.47}$$

With this equation, where t_0=0, $\Delta t_i = 1$ and t_N=t, we can divide the total time interval considered in the equations (2.35), into N-1 intervals:

$$\begin{aligned}\left|\psi_i(t+\Delta t,t)\right\rangle &= \hat{U}(t+\Delta t,t)\left|\psi_i(t)\right\rangle \\ &= \hat{T}_{exp}\left(-\int_{t}^{t+\Delta t}\hat{H}_{KS}(\tau)d\tau\right)|\psi_i(t)\rangle\end{aligned} \tag{2.48}$$

Ehrenfest model equations

In Ehrenfest dynamics the time-step to integrate the electronic and nuclear movement is dictated by the first one. On the other hand, it is not used any electron dynamics to solve BO, since the electronic problem is treated within the time independent Schrödinger equation. So, these equations of motion can be integrated on the time scale given by nuclear motion, and this makes possible to use larger time-steps for dynamics. However, this means that the electronic structure problem has to be solved self-consistently at each molecular dynamics step, while in Ehrenfest dynamics

this is avoided by the possibility of propagating the wavefunction by applying the Hamiltonian to an initial wavefunction.

Ehrenfest TD-DFT MD is one of the several approximations for $\widehat{U}(t+\Delta t,t)$ and it is based on Cank-Nicholson (CN) method:

$$\widehat{U}_{CN}(t+\Delta t,t)=\frac{1-\frac{i}{2}\Delta\widehat{H}_{\mathrm{KS}}(t+\Delta t/2)}{1+\frac{i}{2}\Delta\widehat{H}_{\mathrm{KS}}(t+\Delta t/2)} \tag{2.49}$$

This approximation combined with Runge-Kutta scheme (***29***) consisting in two steps is the one used in the present thesis. Two iterations until convergence of the following integrals are done to solve the TDSE at the middle on each step and at the end of it:

$$\begin{aligned}&|\psi_i^{(n)}(t_0+\Delta t)\rangle=\\&|\psi_i^{(0)}(t_0+\Delta t)\rangle-i\int_t^{t+\Delta t}\widehat{H}_{KS}\left(\{\psi^{(n-1)}(\tau)\},\tau\right)\psi_i^{(n-1)}(\tau)d\tau\end{aligned} \tag{2.50}$$

Summarized, the procedure begins with a first step where for a set of atoms, we read their initial positions $\{\mathbf{r}_o\}$ and velocities $\{\mathbf{v}_o\}$, the basis cut-off and approximation for the v_{XC} (exchange correlation potential), time step, and initial time-dependent $n_o(\mathbf{r},t)$. In our study of double ionization of L-Alanine, we construct this density using all KS orbitals of the neutral molecule except the KS orbital from which we decided to remove two electrons.

Then, we propagate the KS orbitals until the middle of the step (first Runge-Kutta iteration) and once reached that point, we calculate the effective potential $v_{KS}\left(r,t_0+\frac{\Delta t}{2}\right)$. We continue by performing the second Runge-Kutta iteration until the end of the step, using the approximated KS Hamiltonian from the middle of the step.

Then, at the end of the step, we have a new density and using it, we calculate the new forces $\{\mathbf{f}\}$ on the atoms by applying Helmann-Feynman theorem. Finally, by Verlet algorithm (***31***) we update positions and velocities, and this procedures is repeated the number of times needed to reach the total time of simulation needed.

2.5 Modeling the photofragmentation of L-alanine^{2+}

2.5.1 Gaussian Calculations

For these calculations, we used Gaussian09 (***32***) package. We employed standard Pople basis sets (***33-36)*** nd BLYP exchange-correlation functional (***37-41***).

To start our study, we calculate the energy barriers for different fragmentation channels of L-alanine^{2+} and calculate NBO (natural bond orbital) charges. The level of theory used for this calculations is BLYP/6-311 ++G (d,p).

In order to calculate the activation energy of these fragmentations of L-alanine^{2+}

we make scans. A scan consist in increasing systematically the particular bond that is broken and allowing the molecule to relax to the most stable geometry in each step. In this way we are able to know the energy as a function of this particular bond length.

This program was also used to obtain the results needed to calculate Auger spectrum of N 1s of the L-alanine (orbital energies, ionization potentials). In this case, we used two levels of theory: BLYP/6-311 ++G (d,p) and MP2/6-311 ++G (d,p).

To obtain the Auger spectrum, first we calculated the total KER when removing two electrons from any inner orbitals (first and second electron can be removed from the same or different orbital) and then convolute these information.

2.5.2 Setup of CP MD

For both CP MD and TD-DFT MD, we used the latest version 3.15.3 of CPMD code (***42***). This code is a parallelized plane wave/pseudopotential implementation of density functional theory, particularly designed for *ab-initio* molecular dynamics.

Using it, we are able to perform simulations under adiabatic conditions, say using Born-Oppenheimer (BO) MD and Car-Parrinello (CP) MD approximations and furthermore, we are also able to perform simulations of excited states using Ehrenfest TD-DFT MD. In the latter case, we take into account the time dependency of the electronic wavefunction and the non-adiabatic electronic couplings.

For CP MD we use pseudopotentials of the standard Troullier-Martins form (***43***) to replace core electrons and for the valence electron wavefunctions, plane-wave basis set with a cutoff of 70 Ry. In the CP approximation, the electrons are given a fictitious mass and in this way we avoid solving the KS equations each time-step. Due to this approximation, the computational cost is much lower than for TD-DFT MD calculations.

In this case, it is important for the mass assigned to the electrons to be such that it guarantees the adiabaticity. After trying different values of mass with different time steps, we found that the optimal values for our system are: 400 a.u. for the mass, and time step of 1 a.u. (24 as). The optimized cubic cell was of edge length 20 Å.

All simulations have been performed in the NVE ensemble, including the generalized gradient corrections of Becke, Lee, Yang and Parr (BLYP) for the exchange and correlation terms respectively (***37***) (***41***).

2.5.3 Setup for TD-DFT MD

The adiabatic approximation has been assumed. The forces on the nuclei are computed according to the Hellman-Feynman theorem as the analytic derivative of the expectation value of the energy. Here again, the chosen parameters are cutoff of 70 Ry, cubic cell of edge length 20 Å.

Before starting the TD-DFT simulation, we first thermalize the system at 420 K for about 5 ps using CP MD in the NVT ensemble. This step is to supply the molecule the temperature used in experiments. Once this is done, we have a particular conformation with certain coordinates and velocities, and this conformation represents the geometry of neutral L-alanine in equilibrium at the experimental temperature, with

the assumption that the double ionization process is vertical and the geometry of the molecule has no enough time to relax. It is important to remark that although two electrons can be removed from different KS orbitals, in the present study we only analyze those cases in which the ionization is the result of generating two vacancies in a same KS orbital. This particular restriction is imposed because ionizations from different orbitals are unaffordable from computational view point. The implementation of the Ehrenfest dynamics based on TD-DFT used here can handle systems within the local spin density (LSD) approximation, however as the number of spin-orbitals becomes double, the CPU time required increases by 80 %.

To start the fragmentation dynamics, and using the structure of the neutral L-alanine, we build up the electronic density, perform a calculation where all the KS orbitals are considered, except that one from which two electrons are going to be removed.

We said before that in the case of CP MD the time step was 1 a.u., but for TD-DFT MD if we want the total energy of the system (Kohn Sham energy + kinetic energy) to be conserved, we need to use much smaller time step value for the time propagation of the KS orbitals.

When selecting the optimal time-step value to propagate the wavefunction in the TD-DFT MD, the main requirement is the conservation of the total energy. But in practice, it is not absolutely conserved due to numerical errors introduced by the algorithm of propagation. An extra energy introduced by the numerical errors, can give a bias in the results of the simulations. In general, using smaller time steps improves the conservation of the energy but the disadvantage of this is that it increases the computational costs. So, one has to find a compromise between the conservation of energy and the time of simulation.

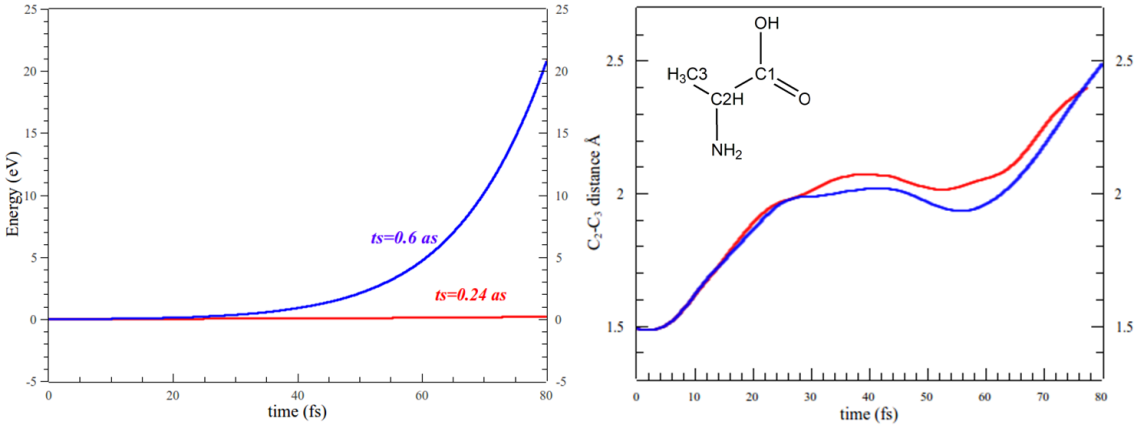

Fig. 2.1(a): Total energy as a function of time for the time step of 0.24 as and the time step of 0.6 as. (b): C_2-C_3 bond length as a function of time.

We selected two different time-steps: 0.01 a.u. (0.24 as) and 0.025 a.u. (0.6 as). Although the values of the bond length obtained by the two time steps are comparable Fig. 2.1(b), the results for time step 0.6 as, are not reliable because the total energy is not conserved. As we show in Fig. 2.1(a), for the time step of 0.24 as, the total variation in the total energy is 0.2 eV while for time step of 0.6 as, the energy increases a lot.

2.5.4 Bader analysis of the charge

When studying fragmentation dynamics, we are interested not only in the broken bonds but also in the charge that each fragment has. Since the atomic charges are not observable, they are not defined by quantum mechanical theory. We find two main ways to make partition of converged electronic density from a quantum calculation between fragments, to assign charges: orbital-based methods and methods based on electrostatic potential or electron density. In the present thesis, to decompose the charge density we use the approach of Bader (***44***) (***45***), based on electron density.

Under this theory, to divide atoms it is used the so-called "zero flux surfaces". A zero flux surface is a 2-D surface on which the charge density is a minimum perpendicular to the surface. Typically in molecular systems, the charge density reaches a minimum between atoms and this is a natural place to separate atoms from each other. The charge enclosed within the Bader volume is a good approximation to the total electronic charge of an atom.

Chapter 3. RESULTS

In this chapter, we present the results of our studies, beginning with non dynamical studies and then continuing with dynamical studies in gas phase: both using CP MD and TD-DFT MD simulations to study the fragmentation of L-alanine^{2+}.

In section 3.1, we give the results of our study for the energy barriers of the fragmentation of L-alanine^{2+} and the charge distribution on the produced fragments. Then, in section 3.2, we show the Auger spectrum for the ionization of N 1s of L-alanine. In section 3.3, we lay out the thermal dissociation of L-alanine^{2+}. Finally, in section 3.4, we make a description of the fragmentation in excited state, when two electrons are removed from KS orbital 6. In each study we make a comparison with experimental data.

In Fig. (3.1) we show the labels used for L-Alanine molecule.

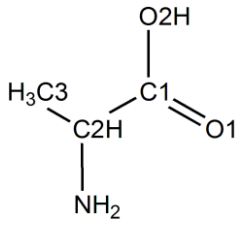

Fig. 3.1: Labels used for atoms in L-Alanine.

3.1 Energy barriers for fragmentation of L-alanine^{2+}

To study different fragmentation channels of doubly-charged L-alanine in triplet state, we use Guaussian09 package to determine energy barriers and charge distribution on the produced fragments. Our study begins with the analysis of the energy barriers for the fragmentation of doubly charged L-alanine in its triplet state, since the triplet alanine^{2+} is 0,33 eV more stable than the singlet one.

Performing this calculation, which consists of elongating a bond in particular and calculating the energy of the geometry in each step, we are able to obtain the energy profile during the fragmentation.

We made two scans. In the first one, we increased systematically the bond between the atoms C_1-C_2. This procedure corresponds to the fragmentation of L-alanine^{2+} leading two fragments: a COOH group and NH_2HC-CH_3 fragment. The energy barrier found for breaking this particular bond is 0.13 eV. As we said before, we are interested not only in the fragments produced, but also in the charge.

For this purpose, we performed a NBO calculation that gives us the charge on each atom at the beginning and at the end of the fragmentation.The result is that each of the fragments is singly charged, as can be seen in Fig. (3.2 a).

The fragmentation channel corresponding to the breaking of C_2-C_3 bond, leads to the formation of a methyl group and NH_2HC-COOH fragment. For the triplet L-alanine^{2+} to be broken in this way, 0.48 eV of energy is needed (see Fig. 3.2 b). About the charge distribution, the methyl group ends up with a charge of 0.6, while the NH_2HC-COOH with 1.4, indicating that each fragment is singly charged.

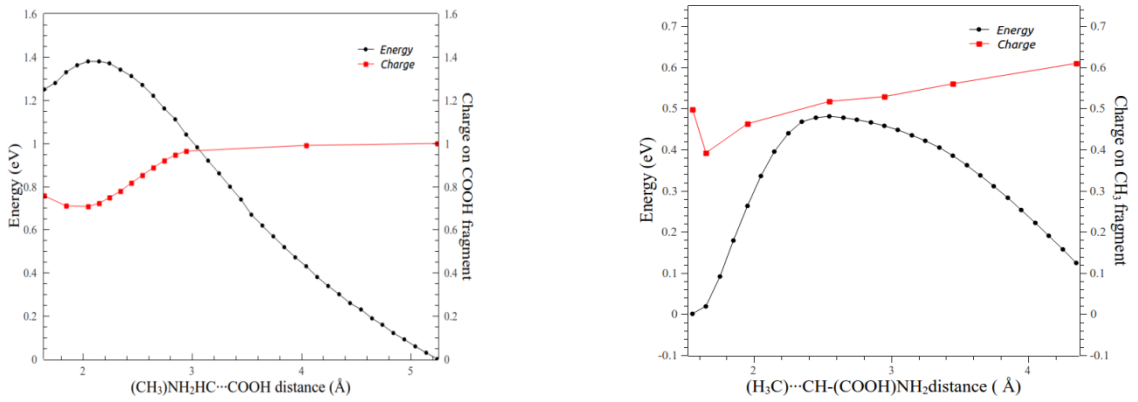

Fig. 3.2: Relative energy and charge on (a) COOH fragment as a function of C_1-C_2 distance and on (b) CH_3 fragment as a function of C_2-C_3 distance.

3.2 Auger Spectrum of L-alanine^{2+}

In the present section we show how we simulated the Auger spectrum corresponding to the ionization of L-alanine on N 1s orbital using all-electron calculations. We make a comparison of our results with the experimental Auger spectrum.

Before showing the results of our simulations, let's explain what the Auger effect is. Auger effect is a physical event that involves three electrons. It starts when a molecule is incised with a certain amount of energy, in particular in our case, with X-rays and removes an electron (called photoelectron) from an inner shell. This vacancy, or hole, increases the energy of the molecule, so the molecule will try to relax from this excited state. In order to do this, a second electron from an upper orbital will fill the hole generated by the first electron, leaving now a hole in its initial position. A third electron, (called Auger electron) will be emitted by energy released by the transition of the second electron, and leave the molecule with a certain kinetic energy. This kinetic energy release (KER) can be measured. At this point, we have two holes in the molecule. It means that the molecule is doubly charged. This process is summarized in the Fig. (3.3):

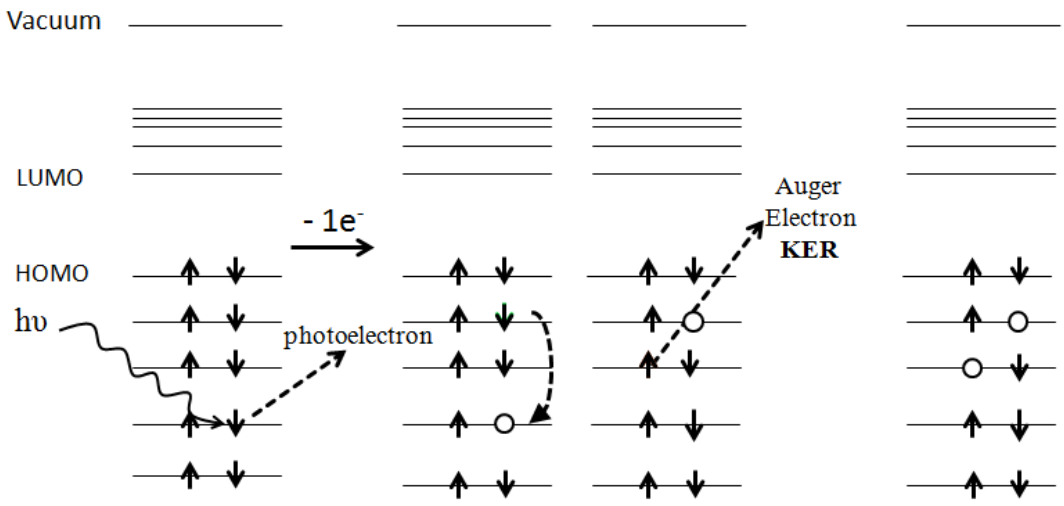

Fig 3.3: Scheme of the Auger process.

Calculation of the Auger spectrum

Although there are more complicated ways of obtaining the kinetic energy of the Auger electron, our goal is to make an estimation using a simpler method, performing all-electron calculations.

For this purpose, we begin with the calculation of the first and second vertical ionization potentials (IP and IP2 respectively).

We use two levels of theory for these calculations: BLYP/6-311++G(d,p) and MP2/6-311++G(d,p). In Fig. (3.4) we see the shape and the energies of the orbitals of the neutral L-alanine calculated using BLYP/6-311++G(d,p).

As we are considering vertical ionization, the geometry used for neutral, singly and doubly charged L-alanine is the same as the optimized geometry of the neutral molecule. Having the energy of these structures and the energy of all the orbitals, we are able to obtain the ionization potentials, which are: IP: 9.15 eV, IP2: 25.24 eV (for

BLYP) and IP: 8.73 eV, IP2: 23.33 eV (for MP2).
Calling *j* the orbital from where the electron that fills the K-hole is decaying, the released energy will have different values. This energy ΔE has the expression:

$$\Delta E^{j}_{decay} = E_{core} - E_j \tag{3.1}$$

E_i and E_j represents in our case the energies of orbitals from L-alanine^{+}.
The energy needed to remove the second electron (*i*) is:

$$\Delta E^{i}_{ioniz} = (E_{HOMO} - E_i) + (IP2 - IP) \tag{3.2}$$

The Auger process only takes place if it is fulfilled the condition:

$$\Delta E^{j}_{decay} > \Delta E^{i}_{ioniz} \tag{3.3}$$

And the kinetic energy of the *i* electron is:

$$E^{ij}_{K} = \Delta E^{j}_{decay} - \Delta E^{i}_{ioniz} \tag{3.4}$$

From these previous expressions, we finally obtain the expression for the total kinetic energy:

$$E^{ij}_{K} = E_{core} - E_j - (E_{HOMO} - E_i) - (IP2 - IP) \tag{3.5}$$

In our case, the K orbital where we make the ionization, is the 1s of the N atom. If we decided for example to ionize on carbon, the result would have not been easy to interpret since the L-Alanine has more than one of those atoms, so we are not able to know the contribution of each of them to the total signal. The same reason holds true with the oxygen atoms.
To obtain the Auger spectrum, we use the equation (3.5) and calculate all possible E^{ij}_{K} values for all the combinations of *i* and *j*, then we get the vertical lines of KER in Fig. (3.5). After this, we make a convolution of these lines of KER to get the intensity of the Auger process as a function of KER.

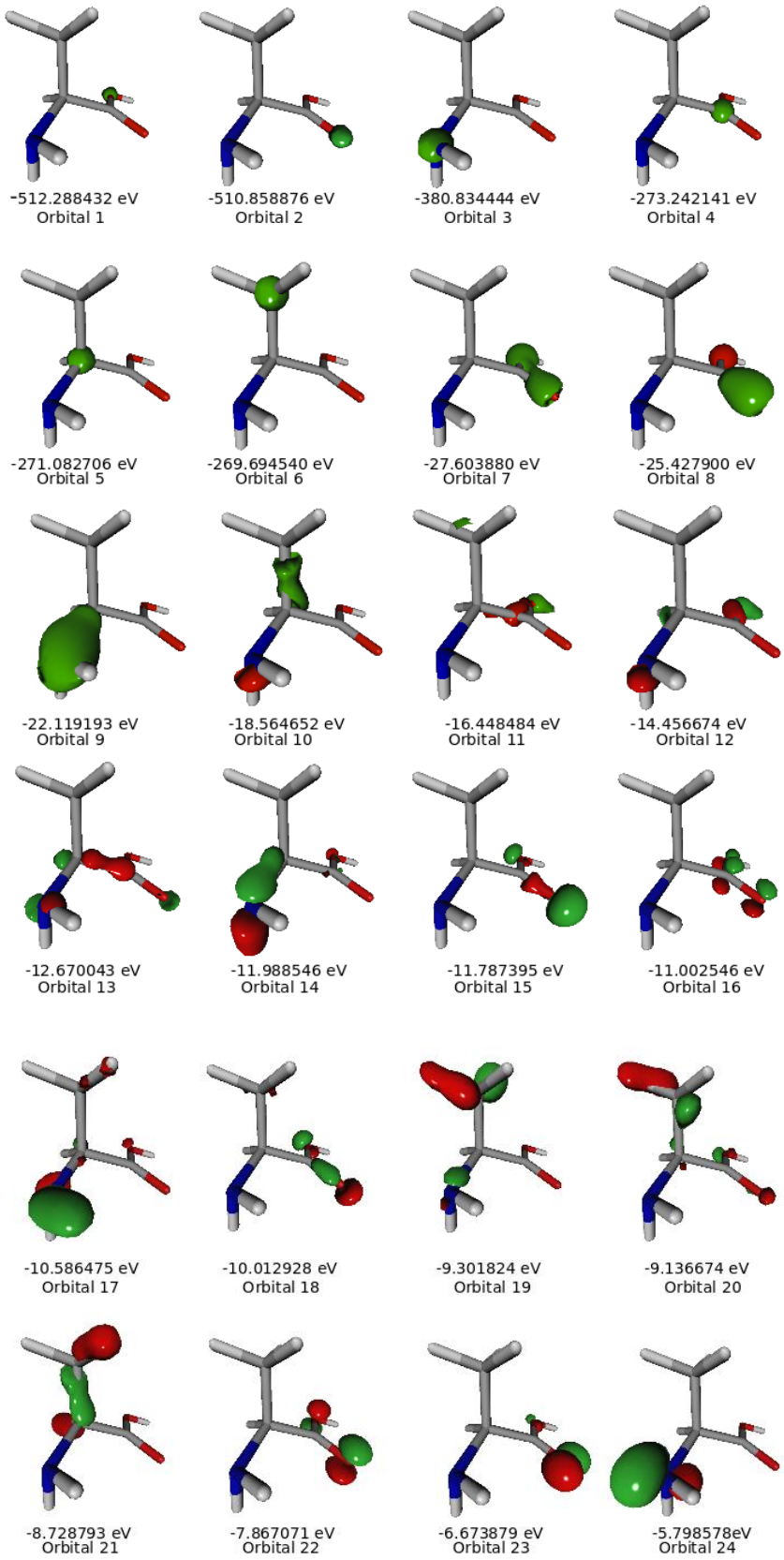

Fig. 3.4: All occupied orbitals of L-alanine calculated at BLYP/6-311++G(d,p) level. Orbitals 1 to 6 correspond to the core orbitals, while from 7 to 24, are valence orbitals.

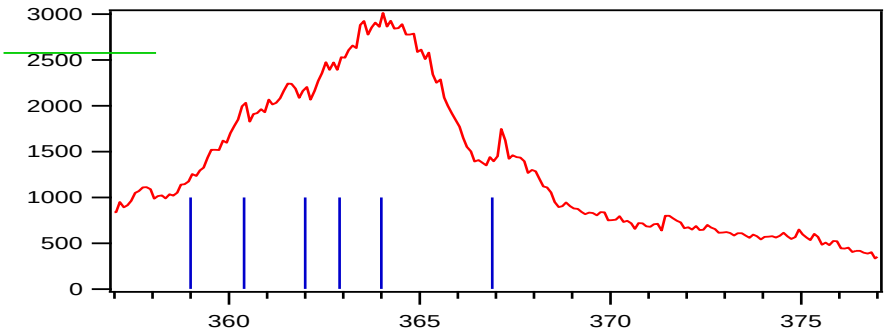

Fig. 3.5: Experimental Auger spectrum of N 1s.

Regarding the simulated Auger spectrum using BLYP/6-311++G(d,p) and MP2/6-311++G(d,p), it is seen that in spite of a shift between them, their shapes are similar. In Fig. (3.5), the shorter vertical lines correspond to all the possible KER (kinetic energy release) values, considering all the combinations for the removal of two electrons (first and second electrons taken from the same or different orbitals). In particular we are interested in the cases corresponding to the situation where both electrons are removed from the same orbital. This assumption is important for the calculation to be computationally affordable. These particular cases are represented by the longer vertical lines. From left to right, the first line represents the KER value for two electrons removed from orbital number 7 which is the first valence orbital, followed by the lines corresponding to excitations from higher orbitals until orbital 24, HOMO orbital. Orbitals from 1 to 6 are core orbitals and the kinetic energies released when removing electrons from them, are around 100 eV, far away from our range of interest. It is worth noting here that in the experiments the energy window or range of energy is around 10 or 15 eV.

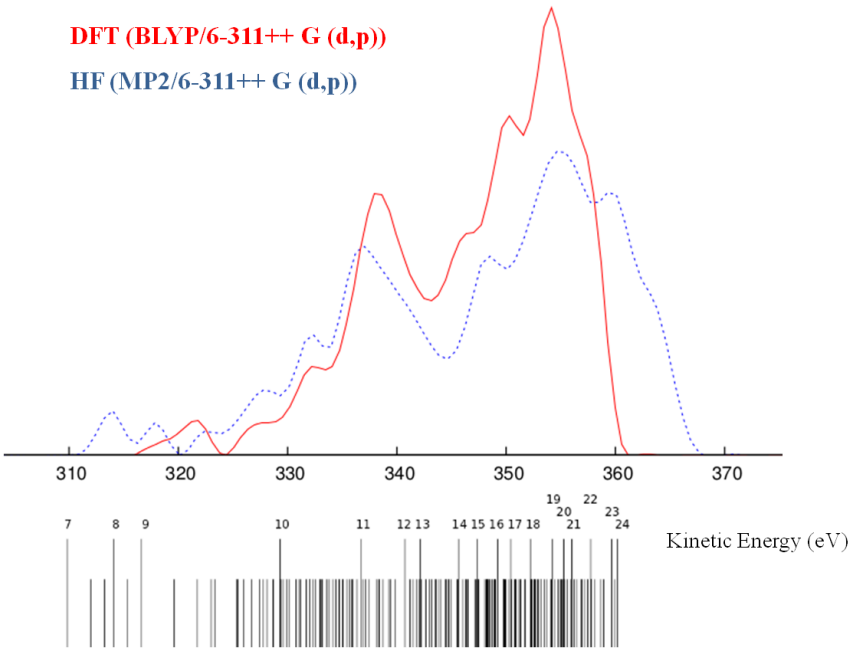

Fig. 3.6: Theoretical Auger spectra for N 1 ionization.

The disadvantage we face here is that N_2 is used for the experiment. As a consequence the experimental Auger spectrum, Fig. (3.5), is dominated by this contamination and is not easy to make comparisons with our theoretical spectra. The red curve in this figure represents the experimental Auger spectrum for the L-alanine and the vertical blue lines correspond to the main lines of N_2 Auger spectrum from literature (***46***).

3.3 Thermal fragmentation of L-alanine^{2+}: a CP MD study

The experiments in gas phase give us information on single collision events and have the advantage, over experiments performed in solution or *in vivo*, of allowing to unambiguously identify fragmentation channels associated with a given molecule and not due to interactions with the environment. When two electrons are removed from a particular shell of the molecule, we create vacancies. This increases the electronic energy of the system, which can relax this excess of energy following a fragmentation process.

We chose L-alanine as a model molecule because is a rather simple molecule that, having no rings, it is supposed to be fragmented in the time of the thesis and also because it was possible to obtain the experimental results from the collaboration group.

In this section we show the results obtained by using Car-Parrinello molecular dynamic method, while the results from TD-DFT molecular dynamics are summarized in the next section. In addition to this, we analyze here the results from experiments performed by people from Turku University, using synchrotron radiation in Max-Lab Sweden.

Results

We have studied several temperatures between 1700 and 3500 K, finally finding that the critical temperature is 1900 K for breaking the molecule. The time scale for the fragmentation is ~ 50 fs. We see this information in Fig. (3.7).

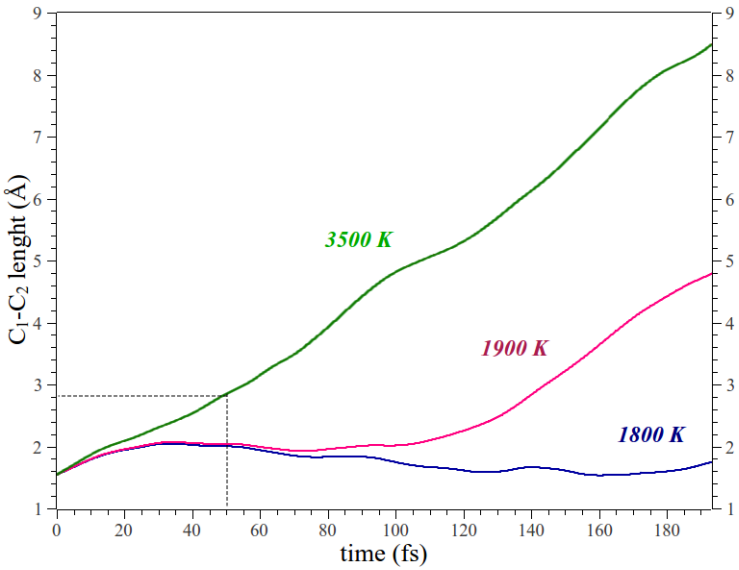

Fig. 3.7: Bond C_1-C_2 distance as a function of time at 1800, 1900 and 3500 K.

Once determined the critical temperature for the fragmentation, we have studied the fragmentation dynamics for certain temperatures. These temperatures used correspond in each case to the energy that would be needed to move the electron from a particular inner orbital to the HOMO orbital. We calculate this thermal energy considering the difference in energy between the considered inner orbital and the HOMO orbital.

We have found that below 11254 K, only the C_1-C_2 bond is broken, leading to two fragments: COOH and $CH_3CH(NH_2)$ with masses 45/44, respectively and charge +1 on each fragment, calculated by Bader analysis.

If we thermalize over 12985 K and until 14472 K, additionally we observe the fragmentation of C_2-N bond. In this case the final fragments are COOH, H_2CCH_2 and NH_2 with masses 45/28/16 respectively. The NH_2 fragment is neutral, while the other two fragments remain having charge almost 1+ each of them.

In Table (3.1) we show the information resulting from dynamical studies in order to be compared with experimental results, Fig. (3.8).

T (K)	KS orbital	Fragment (**mass**) *charge*			Broken bonds
2591	17	COOH (**45**) *0.68*	$CH_3CH(NH_2)$ (**44**) *1.32*		
2693	16	COOH (**45**) *0.84*	$CH_3CH(NH_2)$ (**44**) *1.16*		
3355	15	COOH (**45**) *0.68*	$CH_3CH(NH_2)$ (**44**) *1.32*		
3764	14	COOH (**45**) *0.98*	$CH_3CH(NH_2)$ (**44**) *1.02*		
4222	13	COOH (**45**) *0.98*	$CH_3CH(NH_2)$ (**44**) *1.02*		C_1-C_2
5144	12	COOH (**45**) *0.98*	$CH_3CH(NH_2)$ (**44**) *1.02*		
6307	11	COOH (**45**) *0.96*	$CH_3CH(NH_2)$ (**44**) *1.04*		
8138	10	COOH (**45**) *0.94*	$CH_3CH(NH_2)$ (**44**) *1.06*		
11254	9	COOH (**45**) *0.87*	$CH_3CH(NH_2)$ (**44**) *1.13*		
12985	8	COOH (**45**) *0.92*	H_2CCH_2(**28**) *0.86*	NH_2 (**16**) *0.22*	C_1-C_2; C_2-N
14472	7	COOH (**45**) *0.87*	H_2CCH_2 (**28**) *0.72*	NH_2 (**16**) *0.22*	C_1-C_2; C_2-N

Table 3.1: temperatures, KS orbitals and fragments (with corresponding masses and charges) produced by thermal fragmentation.

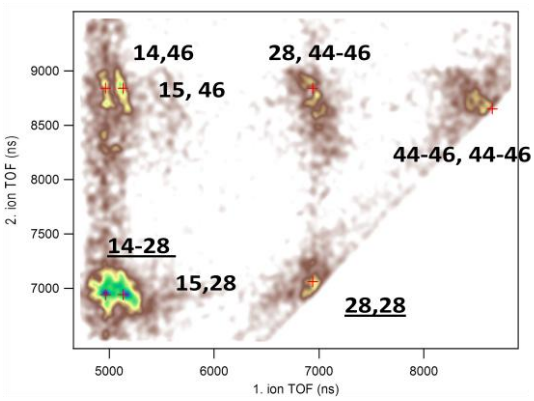

mass	Possible fragments
14	CH_2, N
15	NH, CH_3
28	H_2CCH_2 CO N_2 (contamination)
44	$CH_3CH(NH_2)$
45	COOH
46	HCOOH

Fig. 3.8(a): Experimental results for the ionization of L-Alanine: PEPIPICO map. (b) Possible fragments corresponding to each value of mass.

In the PEPIPICO map, we see signals identified as 44-46/44-46. From the information in the table, we can say that it could correspond to the fragmentation channel observed for temperatures higher than critical temperature and below 11254 K, leading to two fragments with masses 44/45.

On the other hand, the signal of 28, 44-46 could correspond to the masses of fragments obtained at the highest temperatures analysed, 12985 and 14472 K, for which we find three fragments, and two of them that carry the greatest charges having mass of 28/45.

The problem we face here is now again, that the experiment results are contaminated with N_2 signals. So, for example a fragment with mass 28 could correspond either to H_2CCH_2 fragment, or could be a false coincidence, coming from N_2 that has this same value of mass. Analogue reasoning is valid for the path 14-28, since a mass value of 14 could correspond for example to a CH_2 fragment or to a N atom.

For the highest temperature analyed, 14472 K, we show some frames from the dynamics, Fig. (3.9), we see that the first bond broken is the one between C_1-C_2 at ~10 fs.

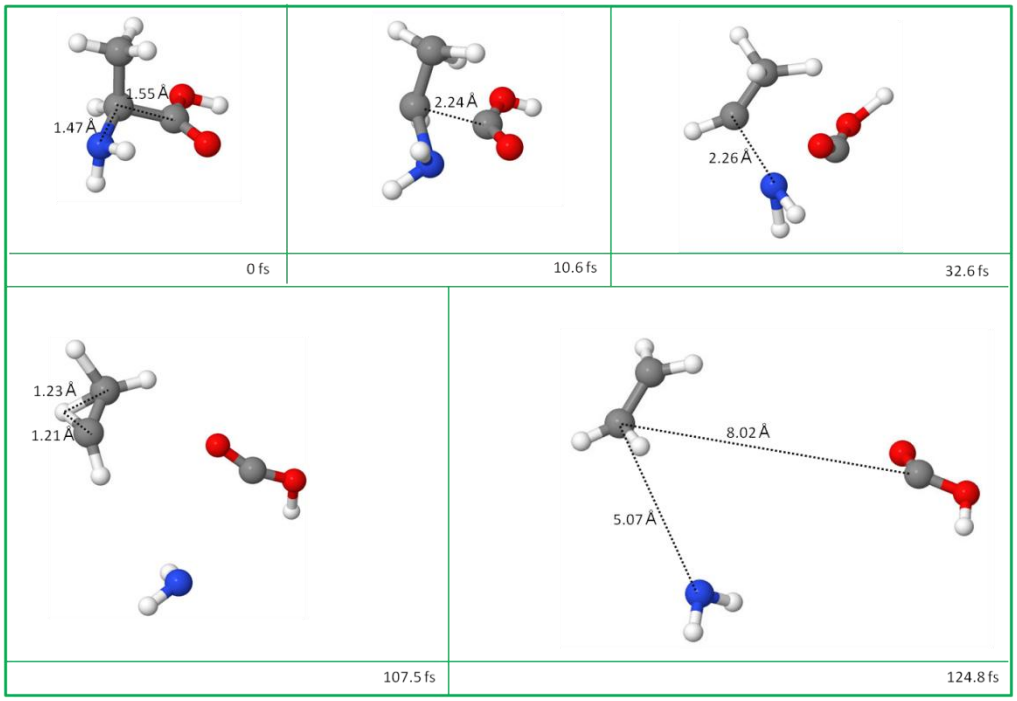

Fig. 3.8: Important changes during the fragmentation dynamics at T= 14472 K.

Then, at ~32 fs, the molecule breaks giving an extra fragment by breaking the bond between C_2-N. Later, at ~107 fs, there is a proton transfer from C_3 to C_2, and finally we see the three fragments with masses 16/28/45. The two charged fragments, those ones with masses 28/45 are also detected in experiment, and there is no signal in the PEPIPICO map for a fragment of mass 16, which is consistent with our result, since the detected NH_2 fragment is neutral.

3.4 Photofragmentation of L-alanine^{2+} in gas phase: a TD-DFT MD study

We use time-dependent DFT molecular dynamics to investigate the fragmentation of L-alanine in excited state: two electrons are removed from an inner shell and the Born-Oppenheimer approximation is not valid any more. We try with this study to interpret the results obtained by ionization of L-alanine using synchrotron radiation.

Concerning the study of fragmentation in excited state, when two electrons are removed from inner shells, what we do first is to build up the wave function and then to perform TD-DFT MD according to the procedures described previously in chapter 2.

The doubly-charged states are obtained by the removal of two electrons from a particular Kohn-Sham (KS) orbital, in our case, from KS6 Fig. (3.9) orbital that have orbital distribution around the nitrogen atom. This is because we are ionizing on N 1s and it is more probable to the hole generated to be filled by another electron in its vicinity.

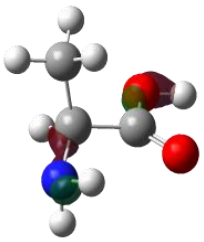

Fig. 3.9: KS orbital 6 of L-alanine.

Results

First, we analyze the evolution of temperature and the Kohn-Sham energy during the fragmentation studied using TD-DFT MD for KS6, and we show it in Fig. (3.10). The simulation starts at 420 K, the temperature used in the experiments. The fluctuations in temperature are due to the exchange of potential energy into kinetic energy.

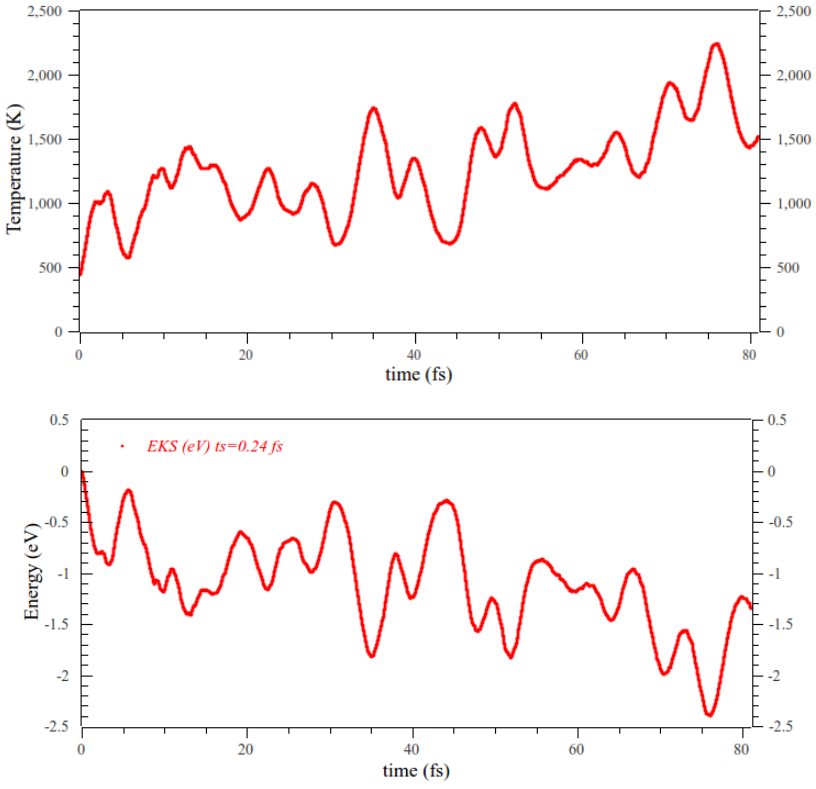

Fig. 3.10: Temperature and Kohn-Sham energy as function of time for KS orbital number 6.

In Fig. (3.12), we see that the distances of bonds C_1-C_2 and C_2-N are fluctuating during all the simulated time but they do not increase significantly. On the other hand, we see an increasing of 1 Å in the length of C_2-C_3 bond, from 1.5 to 2.5 Å. So, this fragmentation channel is expected to lead to two fragments: CH_3 and $(NH_2)CHCOOH$ with masses 15/74. We are extending our simulation in order to see if the C_2-C_3 bond length continues increasing and we are also interested to see if there is further

dissociation, because from experiment it is suggested a fragmentation channel that leads to fragments with masses 15/46.This fragmentation in two steps, is explained by experimentalists when it is seen a pattern with a very steep slope as it is seen in the Fig. 3.14.

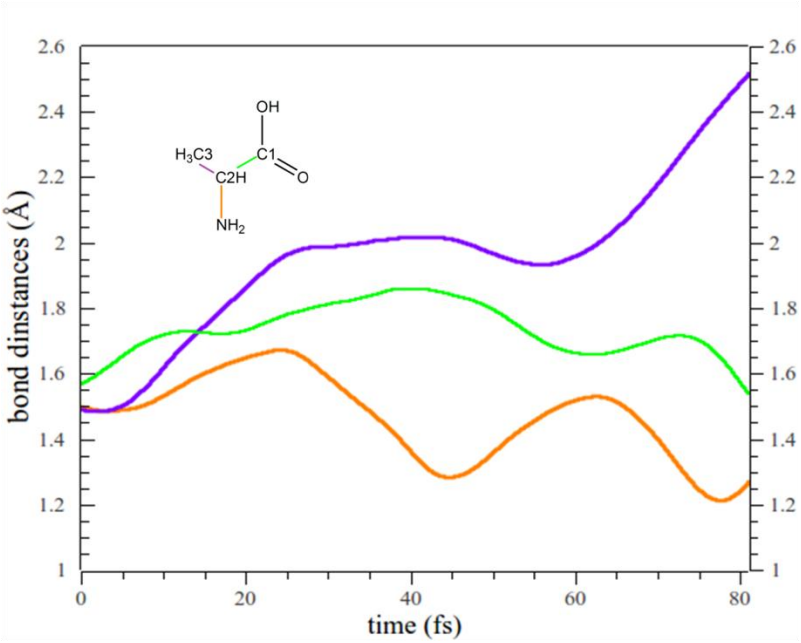

Fig. 3.12: Bond distances as a function of time for KS orbital number 6.

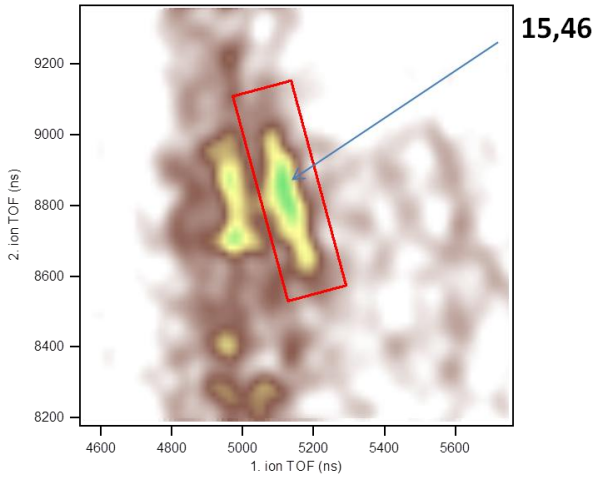

Fig. 3.14: photo-ion photo-ion coincidence map.

As we see, TD-DFT MD simulations increment the information about the fragmentation dynamics of L-Alanine^{2+}. While CP MD simulations at different temperatures predict two different fragmentation channels, where (NH_2)—$CH(CH_3)COOH$ bond and H_3C—$CH(NH_2)COOH$ bond are broken and which have experimental support, TD-DFT MD explain the breaking of H_3C—$CH(NH_2)COOH$.

Chapter 4. CONCLUSIONS

When analyzing the influence of the multiplicity on the stability of doubly charged L-alanine, we see that the triplet state is more stable than the singlet one and is the multiplicity considered for subsequent calculations. The fragmentation channel to break the bond $CH_3(NH_2)HC$—$COOH$ is found to have an energy barrier of 0.13 eV and both produced fragments carry a charge of 1+. On the other hand, to break the H_3C—$CH(NH_2)COOH$ bond an energy barrier of 0.48 eV is needed to be overcome and both produced fragments are singly charged.

The first vertical ionization potential (IP) and second vertical ionization potential (IP2), calculated at two levels of theory are: IP=9.15 eV and IP2=15.24 eV (BLYP/6-311++G(d,p)) and IP=8.73 eV and IP2=23.33 eV ((MP2/6-311++G(d,p)). Based on the calculated the ionization potentials, we calculate the theoretical Auger spectrum for N 1s at the BLYP/6-311++G(d,p) level of theory and it is comparable with the one calculated at the MP2/6-311++G(d,p) level.

We have studied the thermal dissociation of L-alanine^{2+} using CP MD and 1900 K is found to be the minimal temperature needed to be supplied to the system to see any fragmentation. Temperatures higher than this value lead to different fragmentation channels: below 11254 K, only $CH_3(NH_2)HC$—$COOH$ bond is broken leading to two fragments with mass 44/45 and each fragment is singly charged; above this temperature, the energy is enough to break an extra bond: H_2N—$CH(CH_3)COOH$. The masses of the corresponding three fragments are 45/28/16.

Both fragmentation channels are supported by experimental results. In the PEPIPICO map we see the coincidence signal 44/45 supporting the fragmentation channel described for temperatures below 11254 K. We also see a signal corresponding to charged fragments with masses 45/28, supporting our results for temperatures above 11254 K. It is not observed in PEPIPICO map a fragment with mass 16, wich is also consistent with our results, since the predicted NH_2 fragment is neutral.

Results obtained using TD-DFT MD are interesting; we observed the breaking of the H_3C—$CH(NH_2)COOH$ bond, leading to a CH_3 fragment of mass 16, observed also in experiments. We expect to observe further dissociation as suggested by experiments. This fragmentation channel is not observed by using CP MD at any temperature.

Chapter 5. FUTURE WORK

To improve the understanding on the fragmentation dynamics of L-alanine^{2+}, we will continue the simulation for KS orbital 6. We expect a secondary dissociation as suggested by the pattern on the PEPIPICO map corresponding to the masses 15/46 due to its steep slope.

Since the simulation is computationally expensive, we will switch from TD-DFT MD to Born- Oppenheimer MD as long as both methods are giving consistent results.

We have been performing simulations by removing two electrons from KS 11, so we will continue them and compare the results with the PEPIPICO in experiments.

Chapter 6. BIBLIOGRAPHY

1. MacMahon, B. *JNCI J Natl Cancer Inst.* **1962,** *28* (5), 1173.
2. Boice, J. . J. D.; Preston, D.; F. G. Davis, F. G.; Monson, B. B. *Radiation Research* **1991,** *125* (2), 214.
3. Kukk, E.; Sankari, R.; Aksela, H.; Aksela, S. *J. Electron Spectrosc. Relat. Phenom.* **2007,** *151*, 141.
4. Itälä, E.; Kukk, E.; Ha, D. T.; Granroth, S.; Calö, A.; Partanen, L.; Aksela, H.; Aksela, S. *J. Chem Phys.* **2009,** *131*, 114314.
5. Itälä, E.; Ha, D. T.; Kooser, K.; Rachlew, E.; Huels, M. A.; Kukk, E. *J. Chem. Phys.* **2010,** *133*, 154316.
6. Danby, C. J.; Eland, H. D. *Int. J. Mass Spectrom.* **1972,** *8*, 153.
7. Simon, M.; LeBrun, T.; Morin, P.; Lavollée, M.; Maréchal, J. L. *Nucl. Instrum. Methods B* **1991,** *62*, 167.
8. Simon, M.; Morin, P.; Lablanquie, P.; LavollCe, M.; Ueda, K.; Kosugi, N. *Chem. Phys. Lett.* **1995,** *238*, 2.
9. Field, T. A.; Eland, J. H. D. *Meas. Sci. Technol.* **1998,** *9*, 922.
10. Tavernelli, I.; Rohrig, U. F.; Rothlisberger, U. *Mol. Phys.* **2005,** *103* (963).
11. Tavernelli, I. et al. *Chem. Phys. Chem.* **2008,** *9*, 2099.
12. Kohn, W.; Sham, L. *Phys. Rev. 140*, A1133.
13. Tangney, P. *J. of Chem Phys.* **2006,** *124*, 044111.
14. Ha D., T.; Huels, M. A.; Huttula, M.; Urpelainen, S.; Kukk, E. *Physical Review A* **2011,** *84* (3), 033419.
15. López Tarifa, P. et al. *J. Phys.: Conf. Ser.* **2012,** *388*, 102055.
16. Gaigeot, M.; López Tarifa, P.; Martín, F.; Alcami, M.; Vuilleumier, R.; Tavernelli, I.; Hervé du Penhoat, M.; Politis, M. **2010,** *704* (1-3), 45.
17. Ndongmouo-Taffoti, U. F. et al. *Eur. Phys. J. D* **2010,** *58*, 131.
18. Garber, A. J.; Karl, I. E.; Kipnis, D. M. *J. of Biol. Chem.* **1976,** *251*, 851.
19. Alder, B. J.; Wainwright, T. E. *J. Chem. Phys.* **1957,** *27*, 1208.
20. Alder, B. J.; Wainright, T. E. *J. Chem. Phys* **1959,** *31*, 459.
21. Stillinger, F. H.; Rahman, A. *J. Chem. Phys.* **1974,** *60*, 1545.
22. Kresse, G.; Hafner, J. *Phys. Rev. B* **1993,** *47*, 558.
23. Sagui, C.; Darden, T. A. *Annual Rev. of Biophysics and Biomolecular Structure.* **1999,** *28*, 155.
24. Seminario, P. B. a. J. M. *From Classical to Quantum methods*, 1st ed.; Elsevier Science: Netherlands, 1999.
25. Tuckerman, M. E. *J. Phys. Chem. B* **2000,** *104*, 159.
26. Multidimensional Quantum Dynamics, 1. e. (.-V. G. 2. *Multidimensional Quantum Dynamics*, 1st ed.; Wiley-VCH: Germany, 2009.
27. T. Hansson, C. O. a. W. F. V. G. *Current Opinion in Structural Biol.* **2002,** *12* (2), 190.

28. Goldstein, H.; Poole, C.; Safko, J. *Classical Mechanics,* 3rd ed.; Addison Wesley: San Francisco, 2002.
29. Runge, E.; Gross, E. K. U. *Phys. Rev. Lett.* **1984,** *52,* 997.
30. Sakurai, J. *Modern Quantum Mechanics;* Addison Wesley Longman: USA, 1994.
31. Verlet, L. *Phys. Rev.* **1967,** *165* (201).
32. CT, g. I. W. Gaussian 09 Revision A.1., 2009.
33. Binkley, J. S.; Pople, J. A. *J. Am. Chem. Soc* **1980,** *102,* 939.
34. Krishnan, R.; Binkley, J. S.; Pople, J. A. *J. Chem. Phys.* **1980,** *650* (72).
35. Hehre, W. J.; Ditchfiel, R.; Pople, J. A. *J. Chem. Phys.* **1972,** *56,* 2257.
36. Francl, M. M. et al. *J. Chem. Phys.* **1982,** *77,* 3654.
37. Becke, A. D. *Phys. Rev. A* **1988,** *38,* 3098.
38. Gill, P. *Mol. Phys.* **1996,** *89,* 433.
39. Perdew, J. P.; Burke, K.; Ernzerhof, M. *Phys. Rev. Lett.* **1996,** *77,* 3865.
40. Perdew, J. P.; Burke, K.; Ernzerhof, M. *Phys. Rev. Lett.* **1997,** *78,* 1396.
41. Lee, C.; Yang, W.; Parr, R. G. *Phys. Rev. B* **1988,** *37,* 785.
42. CPMD v3.15.3. IBM Corp.; MPI Festkoerperforschung Stuttgart, (1990-2008) (1997-2001).
43. Troullier, N.; Martins, J. L. *Phys. Rev. B* **1991,** *43,* 1993.
44. Bader, R. F. W. *Chem. Rev* **1991,** *91,* 893.
45. Bader, R. F. W. *Atoms in molecules: A quantum theory;* Oxford University Press, 1990.
46. Cryan, J. P. *J. Phys. B: At. Mol. Opt. Phys.* **2012,** *45,* 055601.
47. Schrodinger, E. *Phys. Rev.* **1926,** *28,* 1049.
48. Hohemberg, P.; Kohn, W. *Phys. Rev. B* **1999,** *59,* 7413.